Authors' accepted manuscript
Article published in *Journal of Sound and Vibration*, Volume 547, 17 March 2023, 117541.
Final published version available at https://doi.org/10.1016/j.jsv.2022.117541

Effects of mobility matrices completeness on component-based transfer path analysis methods with and without substructuring applied to aircraft-like components

Simon Prenant[a,*], Thomas Padois[a], Valentin Rolland[a], Manuel Etchessahar[b], Thomas Dupont[a], Olivier Doutres[a]

[a]*Department of Mechanical Engineering, École de technologie supérieure (ÉTS), Montréal, (Qc), H3C 1K3, Canada*
[b]*Bombardier Aerospace, Dorval, (Qc), H4S 1Y9, Canada*

Abstract

Structure borne noise induced by vibrating systems is considered as a major contribution to the noise generated inside vehicles and can be assessed using Transfer Path Analysis (TPA) methods. Their theoretical formulation requires the mobility of either the vibrating system, the receiving structure or the assembly of the two components according to all Degrees of Freedom (DoFs). However, rotational and in-plane DoFs cannot be measured easily and their determination may result in a more complex experimental set-up or an increase in measurement uncertainties. The need for assessing the full mobility matrices thus deserves to be investigated. In this work, the robustness of multiple TPA methods dedicated to the design and validation phases of aircraft light equipment is investigated numerically according to the mobility matrices completeness and by considering several configurations of assemblies (i.e., different active source properties, different numbers of contact points). Numerical models have been developed to simulate a source with controlled vibratory behavior and the spatial averaged mean-square velocity on the re-

*Corresponding author
Email addresses: `simon.prenant@etsmtl.ca` (Simon Prenant), `Thomas.Padois@etsmtl.ca` (Thomas Padois), `Manuel.Etchessahar@aero.bombardier.com` (Manuel Etchessahar), `Thomas.Dupont@etsmtl.ca` (Thomas Dupont), `olivier.doutres@etsmtl.ca` (Olivier Doutres)

ceiving structure is used as an objective indicator of the method's robustness. For proper predictions accuracy, it is shown that the required completeness should account for the terms of highest amplitude and thus depends on the *(i)* TPA method, *(ii)* active behavior of the source and *(iii)* coupling configuration. A completeness involving all the DoFs is generally required for TPA methods based entirely on the mobility of the decoupled components. Otherwise, the omission of rotational or in-plan DoFs could be suitable for TPA methods based on the mobility of the assembly.

Keywords: Structure Borne Noise, Transfer Path Analysis, Component-Based Transfer Path Analysis, Dynamic Substructuring, Uncertainties, Rotational Degree of Freedom

---

Abbreviations

(CB-)TPA	=	(Component-based) transfer path analysis
CB-TPA-DS	=	CB-TPA with dynamic substructuring
DoF(s)	=	Degree(s) of freedom
IDR	=	Interdecile range
RMS	=	Root mean square
-FB	=	pertaining to the blocked forces method
-IS, IS_P	=	pertaining to the *in situ* method
-MI	=	pertaining to the matrix inverse method
-Vf	=	pertaining to the free velocity method

Completenesses

FULL	=	involving all DoFs
OOP	=	involving the out-of-plane DoFs
TDOF	=	involving all translational DoFs
Z	=	involving the z-axis translational DoF

1. Introduction

Multiple vibrating systems (or sources) are integrated in aircraft and can induce annoying noise in the cabin [1, 2]. This noise, so-called structure borne noise, could be mitigated if the vibrating system, receiving structure and interfaces are well designed during the development phase. Work sharing rules are generally such that the vibrating system is designed by a supplier according to the aircraft manufacturer's requirements. In this context, the manufacturer requires suitable methods to predict the structure borne noise during the design phase, but also during the validation phase to ensure the vibroacoustic quality of the systems integrated into the final product.

Source characterization [4], dynamic substructuring [5] and Transfer Path Analysis (TPA) [3] methods have been developed in the last decades in order to perform dynamical analysis and specify proper design guidelines related to noise mitigation. Source characterization refers to methods for assessing intrinsic dynamic properties of the source [4]. Dynamic substructuring refers to a procedure to build the passive dynamic behavior of an assembly from the passive dynamic properties of its decoupled components [5]. TPA refers to methods for analyzing the transmission of mechanical vibrations in assemblies and identifying the origins of noise [3]. TPA methods can be separated into two subgroups: classical TPA and Component-Based TPA (CB-TPA) [3]. Classical TPA is based on the determination of the passive dynamic property of the receiving structure alone (i.e., mobility, vibro-acoustic transfer function) and the forces generated at the interface between the vibrating system and the receiving structure. These forces, so-called operational forces, are an inherent active dynamic property of the assembly (i.e., substituting a component by another changes the operational forces). CB-TPA is based on the characterization of the passive dynamic property of the assembly and the equivalent forces [3]. These forces are an intrinsic property of the source and their determination can be provided by multiple source characterization methods, such as the *in situ* method [6]. Since both classical TPA and CB-TPA methods require a dynamic quantity pertaining to the assembly, they are mainly dedicated for troubleshooting problems on an existing product during the validation phase. In contrast, the joint use of CB-TPA and dynamic substructuring methods, referred to as CB-TPA-DS thereafter, allows assessing the response of the assembly using only intrinsic properties of the decoupled components. CB-TPA-DS is thus well suited for the design phase, but combines the difficulties related to CB-TPA and dynamic substructuring to predict the dynamic of the assembly, making CB-TPA-DS to be considered as the 'Holy Grail' by van der Seijs *et al.* [4].

However, the aforementioned methods are still not widely spread in the industry, partly owing to the experimental limitations [7] and measurement uncertainties [8, 9]. The main source of uncertainties reported in the literature is related to the completeness of the interface description [3, 10] (i.e., the number and nature of DoFs used to model the movement at the contact interface of an assembly or its components). Indeed, a minimum of 6 DoFs are required to constrain all motions of the interface (e.g., 3 DoFs in translation and 3 in rotation at a single point) [15, 37]. However, for time and ease of implementation purpose, rotational DoFs are commonly omitted (two recent standards oversee the application of CB-TPA and CB-TPA-DS methods considering the translational DoFs only, see [7, 12]), leading to the omission of 75% of the terms of the mobility matrices. In some specific cases, this simplification leads to correct predictions [1, 13, 14]. However, some experimental investigations have underlined that including rotational DoFs may improve the prediction accuracy of the DS [15], CB-TPA [16, 17] or CB-TPA-DS [18, 19] methods. The numerical investigations unanimously highlight the importance of considering rotational DoFs for the application of DS [20, 21, 22, 23], CB-TPA and CB-TPA-DS [12] methods. Both numerical and experimental investigations usually focus on the influence of the rotational DoFs omission on the TPA and dynamic substructuring method's robustness (the prediction accuracy associated with a completeness involving translational DoFs only being evaluated by comparison with one associated with a full completeness involving all of the DoFs [15, 17, 18, 19, 20, 21]). On the other hand, the investigations related to the influence of the omission of in-plan DoFs on the TPA and dynamic substructuring method's robustness are scarce [24]. However, the consideration of those DoFs is challenging in the case of a flat and thin receiving structure as commonly encountered in aircraft applications, since such structures prevent the application of in-plan excitations.

Moreover, the benefit of including rotational DoFs is not always found significant [25]. The influence of their omission on the TPA and dynamic substructuring method's prediction is expected to depend on the dynamic behaviors of the considered structure [23, 26]. However, the investigations on the influence of DoFs omission on TPA and dynamic substructuring method prediction are generally conducted on structures with a specific active and passive dynamic behavior. To author's knowledge, the active dynamic behavior is generally not controlled and its influence on TPA methods accuracy has never been investigated. Furthermore, the passive dynamic behavior of the assembly or the components is generally not detailed and its relation with the influence of DoFs omission on TPA methods accuracy has also never been investigated, to the author's knowledge. Finally, the structures are usually academic (beams [22] and plates [20, 21, 23] assemblies) or from the automotive industry [13, 17, 18, 25, 27]). In the specific case of aeronautical-like structures, investigations related to TPA methods applications are scarce.

Finally, the investigations generally focus on a given TPA method. However, the influence of the DoFs omission may depend on the considered method: the influence of the rotational DoFs omission has been evaluated for a classical TPA and a CB-TPA method [27] and for a CB-TPA and a CB-TPA-DS method [12]; in both cases the results suggest that the methods' predictions have different sensitivities to the rotational DoFs omission. This may be explained by the differences between the governing equations of each subgroup of TPA methods.

The objective of this paper is to evaluate the sensitivity of multiple TPA methods to the mobility matrices completeness, considering several configurations of assemblies (i.e., different active source properties, different numbers of contact points). The investigations are numerical and conducted on an academic structure composed of a rigid source attached to a plate, which are designed to mimic the dynamic behavior of an aeronautical hydraulic pump attached to an aircraft structure. Four matrix completenesses are considered in order to evaluate the impact of rotational DoFs omission, as well as in-plane DoFs, and more generally to identify the DoFs with the highest contributions for the dynamic of structures under study. Four active dynamic behaviors of the source are also considered in order to evaluate the impact of the source on the TPA method's prediction accuracy. Only numerical investigations are considered in order to fully control the source active behavior, characterize the dynamic properties according to the 6 DoFs and to avoid the sources of uncertainties other than the completeness of the mobility matrices. The spatial averaged mean-square velocity of the receiving structure is used as the objective indicator. A statistical representation based on boxplots is introduced and used for a global comparison of the predictions accuracy from a TPA method to another.

The remainder of this document is organized as follows. Sect. 2 deals with the theoretical background of classical TPA, CB-TPA and CB-TPA-DS methods. In Sect. 3, the numerical models used for the investigations is presented. In Sect. 4, the passive and active dynamical properties of the assembly and its components are examined in order to provide useful information to interpret the results provided by all the TPA methods of interest. In Sect. 5, the robustness of the TPA methods is investigated according to the completeness of the mobility matrices and considering multiple active behaviors of the source component and coupling configurations with the receiving components (i.e., one and four interface points).

2. Theoretical background

An assembly composed of a vibrating system A and a receiving structure B is schematically presented in Fig. 1. Both components are connected together at point 2 thanks to a rigid and mass-less interface. The origin of vibrations is due to the internal dynamic excitation of the source A, represented by the forces $\boldsymbol{f}_1$ and velocities $\boldsymbol{u}_1$ at location 1. The velocities $\boldsymbol{u}_4$ at locations 4 on the receiving structure induced by the source vibration are used to assess operational or equivalent forces by an inverse method. The velocities $\boldsymbol{u}_3$ at target locations 3 are directly simulated and also predicted using the classical TPA, CB-TPA and CB-TPA-DS methods. Only the velocity normal to the surface of the receiving structure is considered, meaning $\boldsymbol{u}_3 \in \mathbb{C}^{n_3 \times 1}$, where n_3 is the number of target velocity.

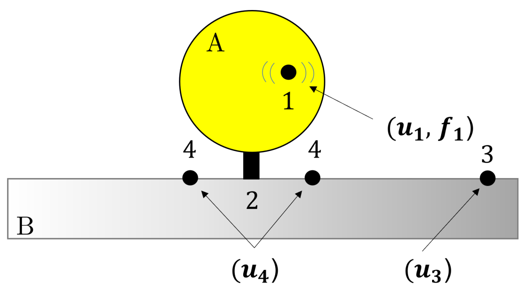

Figure 1: Sketch of the assembly where the source A generates vibration ($\boldsymbol{f}_1$,$\boldsymbol{u}_1$) transmitted through interface 2 to the receiving structure B, where the indicator and target velocities are respectively $\boldsymbol{u}_4$ and $\boldsymbol{u}_3$.

2.1. Mobility definition

The governing equations of the TPA methods are based on admittance (the inverse of the impedance). Admittance corresponds to the ease of movement of a mechanical structure. The admittance Y_{ik} is defined as the ratio between a movement quantity at DoF i denoted u_i and an effort applied at DoF k denoted f_k (assuming a linear behavior of the structure)

$$Y_{ik} = \frac{u_i}{f_k}. \tag{1}$$

Superscripts $(\star)^A$, $(\star)^B$ and $(\star)^{AB}$ are added on Y_{ik} hereafter to indicate the structure or assembly on which the mobility is measured (e.g., Y_{ik}^{A} denotes a mobility pertaining to the source).

Admittance is usually expressed as mobility, namely the movement quantities are homogeneous to translation or rotational velocities and efforts are forces or moments. All terms of Eq. 1 are frequency dependent but the angular frequency (ω) is omitted to lighten notations. The movement and effort being according to six DoFs, the mobility can be expressed in matrix form of size $[6 \times 6]$, as shown in Fig. 2, the rows correspond to the velocities according to each DoF and the columns to the forces and moments (u_i refers to a velocity, θ_i to a rotational velocity, f_k to a force and τ_k to a moment). The completeness is referred as FULL, when all mobility terms are considered in the mobility matrix. Experimentally, the assessment of the FULL completeness is challenging, since it requires the determination of rotational DoFs. Three intermediate completenesses are commonly used, namely Z, TDOF and out-of-plane (OOP), which are depicted in Fig. 2. The Z completeness only involves the term $Y_{u_z f_z}$, related to the velocity and force along the z-axis. The TDOF completeness only involves the terms related to the translational DoFs. Both Z and TDOF completenesses are usually used for experimental purposes because they require only an impact hammer and accelerometers. The OOP completeness involves terms related to the z-axis TDOF and the x- and y-axis rotational DoFs and is well suited for describing the bending motion [34]. The OOP completeness is easier to access experimentally than the FULL completeness, but still requires an indirect method for the determination of rotational DoFs, which may be another source of uncertainties [35].

The number of DoFs considered is referred thereafter to the variable n_2 (i.e., depending on the completeness chosen, $n_2 = 1$, 3 or 6 for a single interface point and $n_2 = 4$, 12 or 36 for four interface points).

2.2. TPA-MI, CB-TPA and CB-TPA-DS methods

The classical TPA methods allow for predicting the target velocity $\boldsymbol{u}_3$ based on the transfer mobility of the receiving structure $\mathbf{Y}_{32}^{B}$ (where $\mathbf{Y}_{32}^{B} \in \mathbb{C}^{n_3 \times n_2}$) and operational forces $\boldsymbol{g}_2^{B}$ (where $\boldsymbol{g}_2^{B} \in \mathbb{C}^{n_2 \times 1}$)

$$\boldsymbol{u}_3 = \mathbf{Y}_{32}^{B} \boldsymbol{g}_2^{B}. \tag{2}$$

The operational forces can be provided by the transfer mobility of the receiving structure $\mathbf{Y}_{42}^{B}$ (where $\mathbf{Y}_{42}^{B} \in \mathbb{C}^{n_4 \times n_2}$, n_4 being the number of indicator

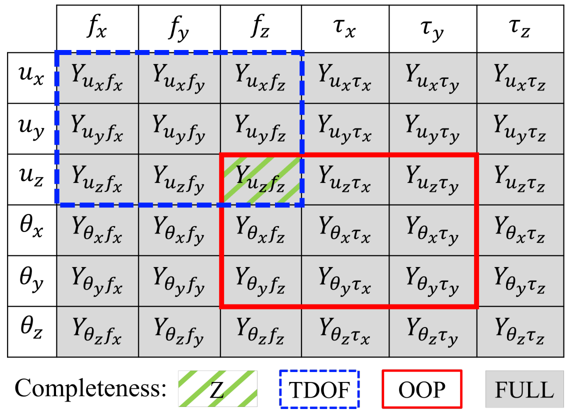

Figure 2: Mobility matrix: depiction of the Z, TDOF, OOP and FULL completenesses (color online).

DoFs) and the indicator velocities $\boldsymbol{u}_4^{AB}$ (where $\boldsymbol{u}_4^{AB} \in \mathbb{C}^{n_4 \times 1}$) when the source is turned on

$$\boldsymbol{g}_2^B = (\mathbf{Y}_{42}^B)^+ \boldsymbol{u}_4^{AB}, \tag{3}$$

where $(\star)^+$ denotes the Moore-Penrose inverse [29]. The operational forces can also be provided by the direct mobility $\mathbf{Y}_{22}^B$ (where $\mathbf{Y}_{22}^B \in \mathbb{C}^{n_2 \times n_2}$). In this work, the classical TPA method based on Eqs. 2 and 3 is called Matrix Inverse (MI) and referred to as TPA-MI in the following.

As mentioned previously, Component-Based TPA (CB-TPA) methods allow predicting the target velocity based on the transfer mobility of the assembly $\mathbf{Y}_{32}^{AB}$ (where $\mathbf{Y}_{32}^{AB} \in \mathbb{C}^{n_3 \times n_2}$) and equivalent forces $\boldsymbol{f}_2^{eq}$ (where $\boldsymbol{f}_2^{eq} \in \mathbb{C}^{n_2 \times 1}$) [3] from

$$\boldsymbol{u}_3 = \mathbf{Y}_{32}^{AB} \boldsymbol{f}_2^{eq}. \tag{4}$$

The equivalent forces are intrinsic properties of the source and can be determined by several source characterization methods. The equivalent forces correspond to the blocked forces $\boldsymbol{f}_2^{bl}$ (where $\boldsymbol{f}_2^{bl} \in \mathbb{C}^{n_2 \times 1}$)

$$\boldsymbol{f}_2^{eq} = \boldsymbol{f}_2^{bl}, \tag{5}$$

which can be measured using an infinitely stiff receiving structure. CB-TPA based on blocked forces is referred to as CB-TPA-FB hereafter. To avoid the need of such an impracticable receiving structure, the equivalent forces may be assessed by the "free velocity" or "*in situ*" methods [6]. The free velocity method consists in suspending the source so as to measure the direct mobility $\mathbf{Y}_{22}^{A}$ at the interface point (where $\mathbf{Y}_{22}^{A} \in \mathbb{C}^{n_2 \times n_2}$) as well as the free velocity $\boldsymbol{u}_2^{free}$ (where $\boldsymbol{u}_2^{free} \in \mathbb{C}^{n_2 \times 1}$) when the source operates. The equivalent forces are given by

$$\boldsymbol{f}_2^{eq} = (\mathbf{Y}_{22}^{A})^{-1} \boldsymbol{u}_2^{free}. \tag{6}$$

CB-TPA based on this method is referred to as CB-TPA-Vf hereafter. With the *in situ* method, the source is coupled to a test bench denoted P. Then, the equivalent forces are provided by the transfer mobility $\mathbf{Y}_{42}^{AP}$ (where $\mathbf{Y}_{42}^{AP} \in \mathbb{C}^{n_4 \times n_2}$) and indicator velocities $\boldsymbol{u}_4^{AP}$ (where $\boldsymbol{u}_4^{AP} \in \mathbb{C}^{n_4 \times 1}$):

$$\boldsymbol{f}_2^{eq} = (\mathbf{Y}_{42}^{AP})^{+} \boldsymbol{u}_4^{AP}. \tag{7}$$

CB-TPA based on this method is referred to as CB-TPA-IS hereafter when the test bench corresponds to the receiving structure ($P = B$) and CB-TPA-IS$_\mathrm{P}$ otherwise ($P \neq B$).

The mobility of the assembly ($\mathbf{Y}_{32}^{AB}$) is then expressed from the mobilities of the decoupled components ($\mathbf{Y}_{22}^{A}$, $\mathbf{Y}_{22}^{B}$ and $\mathbf{Y}_{32}^{B}$) thanks to the dynamic substructuring procedure. The joint use of CB-TPA and dynamic substructuring allows predicting the target velocity $\boldsymbol{u}_3$ by means of the mobility of both decoupled components and the equivalent forces according to

$$\boldsymbol{u}_3 = \mathbf{Y}_{32}^{B} (\mathbf{Y}_{22}^{A} + \mathbf{Y}_{22}^{B})^{-1} \mathbf{Y}_{22}^{A} \boldsymbol{f}_2^{eq}, \tag{8}$$

and is referred to as CB-TPA-DS hereafter.

To sum up, nine methods are investigated in this work, namely: the TPA-MI, four CB-TPA (FB, Vf, IS, IS$_\mathrm{P}$) and four CB-TPA-DS (FB, Vf, IS, IS$_\mathrm{P}$) methods, which are summarized in Tab. 1.

Each term of the mobility matrices ($\mathbf{Y}_{22}^{A}$, $\mathbf{Y}_{22}^{B}$, $\mathbf{Y}_{32}^{AB}$, ...), the free velocities ($\boldsymbol{u}_2^{free}$) and blocked forces ($\boldsymbol{f}_2^{bl}$) are determined numerically according to the six DoFs (translations and rotations). The dimensions of these quantities are then adjusted according to the considered completeness (by truncating row or columns) and are used to predict the target velocity $\boldsymbol{u}_3$. This prediction is then compared to a reference, directly determined from the numerical model.

Method	Target prediction	Active property	Acronyms
TPA	$\boldsymbol{u}_3 = \mathbf{Y}_{32}^{B} \boldsymbol{g}_2^{B}$	$\boldsymbol{g}_2^{B} = (\mathbf{Y}_{42}^{B})^{-1} \boldsymbol{u}_4^{AB}$	-MI
CB-TPA	$\boldsymbol{u}_3 = \mathbf{Y}_{32}^{AB} \boldsymbol{f}_2^{eq}$	$\boldsymbol{f}_2^{eq} = \boldsymbol{f}_2^{bl}$	-FB
		$\boldsymbol{f}_2^{eq} = (\mathbf{Y}_{22}^{A})^{-1} \boldsymbol{u}_2^{free}$	-Vf
CB-TPA-DS	$\boldsymbol{u}_3 = \mathbf{Y}_{32}^{B} (\mathbf{Y}_{22}^{A} + \mathbf{Y}_{22}^{B})^{-1} \mathbf{Y}_{22}^{A} \boldsymbol{f}_2^{eq}$	$\boldsymbol{f}_2^{eq} = (\mathbf{Y}_{42}^{AB})^{+} \boldsymbol{u}_4^{AB}$	-IS
		$\boldsymbol{f}_2^{eq} = (\mathbf{Y}_{42}^{AP})^{+} \boldsymbol{u}_4^{AP}$	-IS$_{\mathrm{P}}$

Table 1: Summary of the considered TPA methods.

3. Numerical model

3.1. Geometry and materials

The assembly is composed of a vibrating bloc as a source (A) and a plate as a receiving structure (B). The assembly and the components are shown in Fig. 3. The aircraft-like source is a cube in aluminum with 100 mm side, in order to model an aeronautical hydraulic pump. The aircraft structure is modelled by a plate, in agreement with current practices [2, 30], and is made of aluminum. Although idealized, this modelization allows an intuitive understanding of the dynamic behavior of the receiving structure. The relevance of this modelization is discussed in Appendix D, where mobilities of the modeled structures are compared to measurements performed on industrial aeronautical structures. The dimensions of the plate used as receiving structure B are $1371,6 \times 965,2 \times 3$ mm^3. The test bench P required for the CB-TPA-IS$_{\mathrm{P}}$ method is a steel plate with same dimensions as the receiving structure B but with a thickness of 4,8 mm. This test bench P is inspired by the test bench used in reference [1]. The indicator points are positioned (4) crosswise and located 20 mm from the center of the interface point (2), as shown in Fig. 3. Translational velocities only are considered at the indicator points (i.e., n_4=12 or 48 respectively for the single and four interface points assemblies). Additional simulations have been performed to investigate the effect of the position of the indicator points on TPA's predictions and showed no effects (results are not presented here for conciseness). This is attributed to the absence of uncertainty other than the omission of DOFs[1].

[1]For experimental investigations the indicator points should be positioned at a reasonably close distance from the interface point to ensure a correct signal-to-noise ratio (see reference [31] for more details).

The material properties of each component are given in Tab. 2.

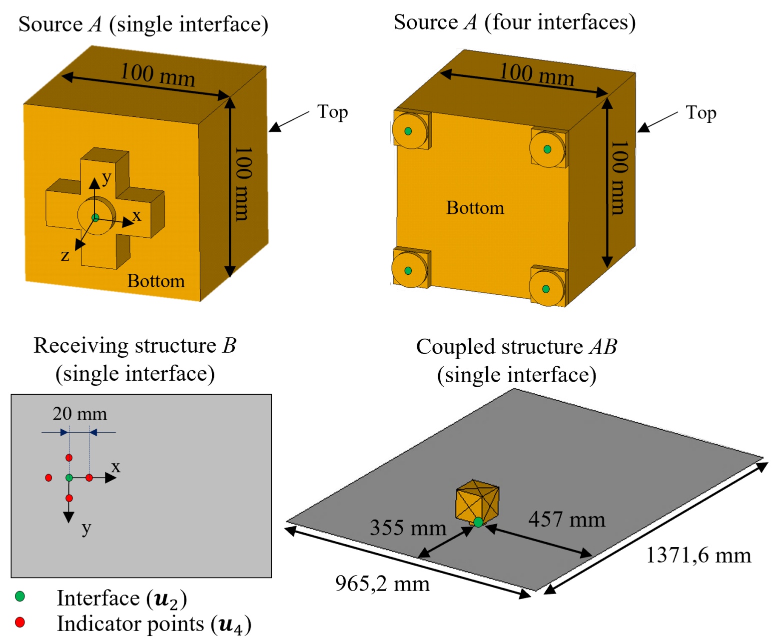

Figure 3: Geometries of the source A, receiving structure B (single interface point configuration) and assembly AB (single interface point configuration).

	Source A	Receiving structure B	Test bench P
Material	Aluminum		Steel
Young's modulus [GPa]	65,6		200
Density [kg/m^3]	2700		7506
Poisson's coefficient	0,33		0,33
Damping ratio	0,5%		0,5%
Dimensions [mm^2]	100×100	$1371,6 \times 965,2$	$1371,6 \times 965,2$
Height/thickness [mm]	125	3	$4,8$

Table 2: Model properties.

Two coupling configurations are considered, the first involving a single interface point, the second involving four interface points. The single interface point configuration allows a simple approach to understand the dynamics at the coupling interface. For this configuration, the computations have been done for three different locations of the source on the plate and have led to similar observations. The four interface points configuration implies interplay between the four interface points and is thus intended to be more realistic of the assembly of an aeronautical hydraulic pump with an aircraft-like structure. In the case of the four interface points structure, the spacing between the interfaces is designed based on a measurement on a real aeronautical hydraulic pump.

3.2. Boundary conditions and loadings

Free and clamped boundary conditions are respectively applied at the interface (point 2) of the source to compute its active properties $\boldsymbol{u}_2^{free}$ and $\boldsymbol{f}_2^{bl}$. Clamped boundary conditions are imposed at the edges of both the plates B and P. For the assemblies, components are hard-mounted without friction thanks to a circular interface with a radius of 10 mm.

The multiple active dynamic behaviors of the source are modelled by applying various loading ($\boldsymbol{f}_1$) at the center of three faces of the cube to the points PX, PY and PZ, as shown in Fig. 4. The forces and moments are applied along the normal direction to the faces. Four excitations are considered, namely Excitation#1 to Excitation#4 and the corresponding amplitude of the three forces and three moments are given in Tab. 3.

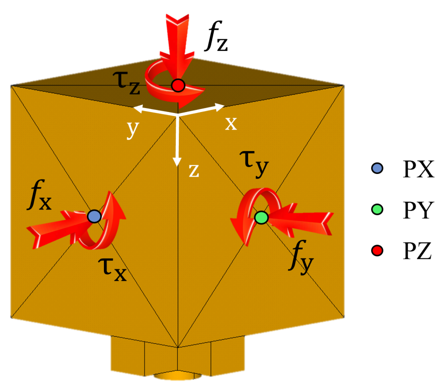

Figure 4: Implementation of the active dynamic behavior of the source.

Excitation#1 considers a force of 1 N applied on PZ and thus is expected to have a simple dynamic behavior mainly in translation along the z axis.

	f_x [N]	f_y [N]	f_z [N]	τ_x [N.m]	τ_y [N.m]	τ_z [N.m]
Excitation#1	10^{-4}	10^{-4}	1	10^{-4}	10^{-4}	10^{-4}
Excitation#2	10^{-1}	10^{-1}	1	10^{-4}	10^{-4}	10^{-4}
Excitation#3	10^{-4}	10^{-4}	1	10^{-2}	5.10^{-3}	10^{-4}
Excitation#4	10^{-4}	10^{-4}	1	10^{-1}	10^{-1}	10^{-4}

Table 3: Details of the loading applied on the cube.

This excitation could be reproduced experimentally using a shaker or instrumented hammer. Excitation#2 is similar to Excitation#1 but two forces of 10^{-1} N are applied on PX and PY. It is expected that the forces applied along x and y generate more complex equivalent forces at the interface ($\boldsymbol{f}_2^{eq}$) due to the lever arm between points PX, PY and interface. Excitation#3 considers a force of 1 N applied on PZ, a 1.10^{-2} N.m moment acting about PX and a 5.10^{-3} N.m moment acting about PY. This set of internal efforts is inspired by the dynamic behavior of an axial piston pump (i.e., a pumping motion and two out-of-plane moments due to piston movements) [33]. Excitation#4 is similar to Excitation#3 but a 1.10^{-1} N.m moment acting about PX and PY. This set Excitation#4 is expected to have the most complex dynamic behavior. For each excitation, a residual value of 10^{-4} N or N.m is applied along the inactive direction in order to avoid singularities.

3.3. Finite element modeling

The numerical model is developed with ANSYS® APDL 19.2. The simulations have been performed using a complete resolution [32] (i.e., without modal summation) in the frequency range 40-3000 Hz with a 2 Hz frequency step.

The source A is meshed with 19 085 solid linear elements (SOLID73) having 6 DoFs/node (16 525 elements for the 4 interface points source). These elements have been involved only for the purpose of computing dynamic quantities pertaining to rotational DoFs, without indirect method. Otherwise, elements having less DoFs per node (e.g., SOLID183) could be used for time-efficient computations, conjointly with an indirect method or a pilot node for computing the rotational dynamic quantities. The geometry of both components B and P is meshed with 15 954 shell linear elements (SHELL63) having 6 DoFs/node (13 770 elements for the 4 interface points plate). TARGET170 and CONTA174 elements are used at the contact interface of the components to ensure the rigid coupling. A mesh convergence study has been done to ensure that results are mesh-independent.

3.4. Computation of vibratory indicators

The Root Mean Square (RMS) of the mobilities and the equivalent forces is used to identify the DoFs governing the dynamic behavior of the assembly and its components in a readable way, despite the large number of terms (see Sect. 4). The RMS value of each term of the mobility matrices and equivalent force vectors is computed according to

$$X_{RMS} = \sqrt{\frac{1}{N}\sum_{n=1}^{N} |X(n)|^2}, \tag{9}$$

where X corresponds to a dynamic quantity, N to the number of frequency bins (i.e., here N=2960) and $|\star|$ to the l_2-norm of $(\star)$.

The various TPA methods of interest are used to predict n_3=1408 target velocities u_3 uniformly distributed on an area S of the receiving structure. The Spatial Averaged Mean-Square Velocity $\langle u_3^2 \rangle$ is then computed according to

$$\langle u_3^2 \rangle = \frac{1}{2S} \iint_S |\boldsymbol{u}_3(x,y)|^2 \, dS \tag{10}$$

and $\langle u_3^2 \rangle$ is used as an objective indicator for evaluating the robustness of the TPA methods. This choice is substantiated since this target is directly related to the equivalent radiated power of a thin structure [34, 36]. As shown in Appendix A, going through spatial averages allows a better evaluation of TPA method's robustness since it avoids a dependence of the observation point (i.e., the location of the DoF target u_3).

The evaluation of TPA method's robustness involves the comparison of methods predictions together with a reference obtained from a direct simulation of the operating source attached to the receiving structure. A qualitative comparison of the predicted and reference frequency dependent $\langle u_3^2 \rangle$ for each configuration would be too demanding due to the large number of configurations (4 excitations, 4 matrix completenesses and 9 TPA methods which corresponds to a total of 144 scenarios for each of the single and four interface points assemblies) and the amount of data in the considered frequency range (40-3000 Hz). Two objective metrics based on the frequency response assurance criterion [16] [28] and the RMS [19] were used in previous works.

However, these metrics are too synthetic (i.e., a frequency-dependent prediction is synthesized by a single value). For this reason a representation using boxplot is introduced and used in this document.

The difference between the predicted and reference $\langle u_3^2 \rangle$ is computed at each frequency bin for each configuration and the statistical parameters of this frequency-dependent function are computed and displayed using a boxplot. The frame of the boxplot limits the values of the first and ninth deciles. Its size, called Inter Decile Range (IDR), allows to represent the dispersion of 80% of the values around the median and thus is the most well-suited indicator to quantify the robustness of a method prediction. The whiskers limit the minimum and maximum values. A boxplot with small IDR, a median value equal to zero and small whiskers is associated to the most desirable scenario for which the $\langle u_3^2 \rangle$ is correctly predicted by a given TPA method and associated mobility matrix completeness (i.e., the model error is low). A boxplot with small IDR, a median value equal to zero but with large whiskers corresponds to a $\langle u_3^2 \rangle$ prediction considered globally correct but with local discrepancies (e.g., the vibratory behavior of the receiving structure is poorly captured at some specific frequency bands such as antiresonance and/or resonance frequencies). This latter case may not be problematic for a broadband source but undesirable in the case of a tonal source, since the operating frequency of the source may coincide with a strong local discrepancy. Three examples are detailed in Appendix B in order to illustrate the boxplot representations associated with a perfect prediction and two predictions leading to large whiskers but small IDR. The worst scenario occurs for a boxplot with large IDR and whiskers. It corresponds to a $\langle u_3^2 \rangle$ prediction which varies a lot around the median value (i.e., the predicted SAMV is considerably different from the reference in the whole frequency range). In this specific case, the median and the arithmetic mean may provide additional information, but should be analyzed with caution. Indeed, their values can be close to 0 and centered on the boxplot frame, when over- and under-estimations compensate for each other (which is common when prediction inaccuracies are related to frequency-shifted peaks). Consequently, a median of the boxplot close to zero is a necessary but not sufficient condition to conclude about the accuracy of a TPA method. Furthermore, an off-centering of the median value in the boxplot frame or different values between the median and mean values indicates an unbalance between the over- and under- estimations, which may be induced by particular phenomena located at a specific frequency band. Illustrative examples are provided and analyzed in section 5.1.

4. Identification of the DoFs governing the dynamic behavior of components and assemblies

This section examines the passive and active dynamical properties of the assembly (single interface point configuration) and its components in order to provide useful information to interpret the results provided by all the TPA methods of interest (i.e., TPA-MI, CB-TPA and CB-TPA-DS).

4.1. Mobility

The RMS value (see Eq. 9) of all mobility terms of $\mathbf{Y}^A_{22}$ is represented in Fig. 5.a). It is shown that the terms with the highest amplitude are located on the diagonal and on an "anti-diagonal". According to Fig. 5, only the FULL completeness allows to accounting for all of these terms. The RMS values of the receiving structure mobility matrix at interface 2, $\mathbf{Y}^B_{22}$, are represented in Fig. 5.b). As expected, the dynamic behavior of the plate is mainly governed by bending (i.e., the out-of-plane (OOP) completeness). The RMS values of the assembly transfer mobility $\mathbf{Y}^{AB}_{3u_z2}$, and related to a single randomly chosen target point 3, are shown in Fig. 5.c). Only the values related to the z-axis velocity are shown, since they are the only ones required for the prediction of $\boldsymbol{u}_3$. It highlights a dynamic behavior governed by OOP completeness. While the passive dynamic behavior of the assembly is globally bending-governed, modes with more complex shapes appear at high frequencies and are referred to as "complex shape" modes in the following. To illustrate this, the frequency-dependent mobility magnitudes are shown in Fig. 6. The mobilities associated to the OOP completeness (i.e., $Y^{AB}_{3u_z2f_z}$, $Y^{AB}_{3u_z2\tau_x}$ and $Y^{AB}_{3u_z2\tau_y}$) dominate up to 2000 Hz. The modes in this frequency range follow the bending deformation pattern of the plate (Fig. 7).a)). Above 2000 Hz, complex shape modes appear. As shown in Fig. 7.b), their patterns involve significant movements in translation of the source in the x- and y-axis direction. These modes result from the interaction of the source mobility with the first traction-compression modes of the plate. Consequently, the amplitude of the mobilities $Y^{AB}_{3u_z2f_x}$ and $Y^{AB}_{3u_z2f_y}$ increases locally and are similar or higher in amplitude in this frequency range compared with $Y^{AB}_{3u_z2f_z}$.

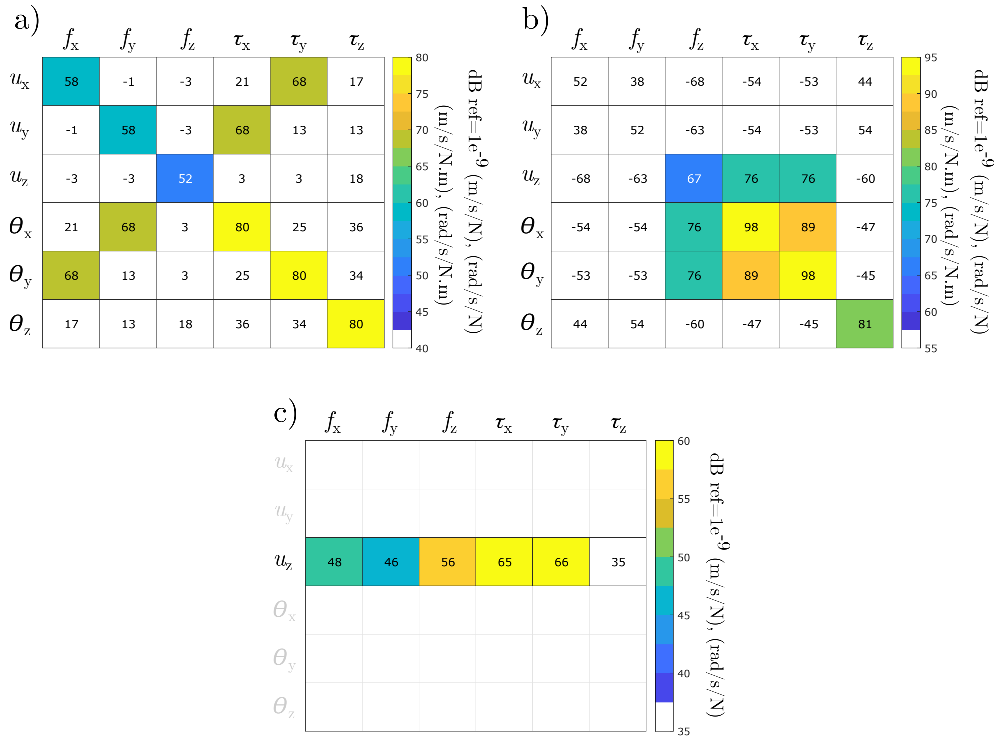

Figure 5: RMS values of a) $\mathbf{Y}_{22}^{A}$, b) $\mathbf{Y}_{22}^{B}$ and c) $\mathbf{Y}_{32}^{AB}$ related to a single randomly chosen target point (color online).

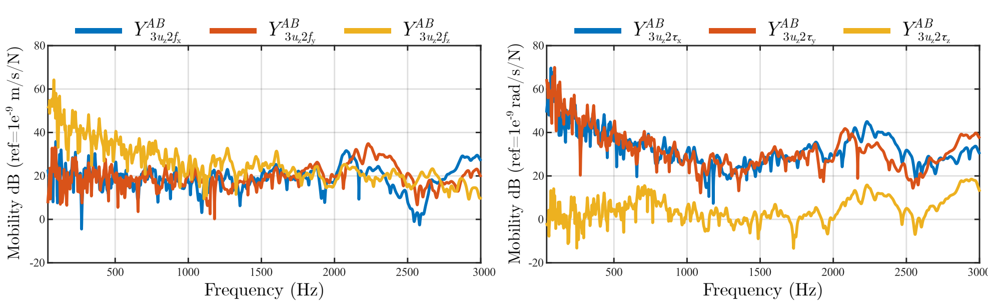

Figure 6: Magnitude of mobility $Y_{3u_z2}^{AB}$ versus frequency pertaining to the single interface point configuration assembly (color online).

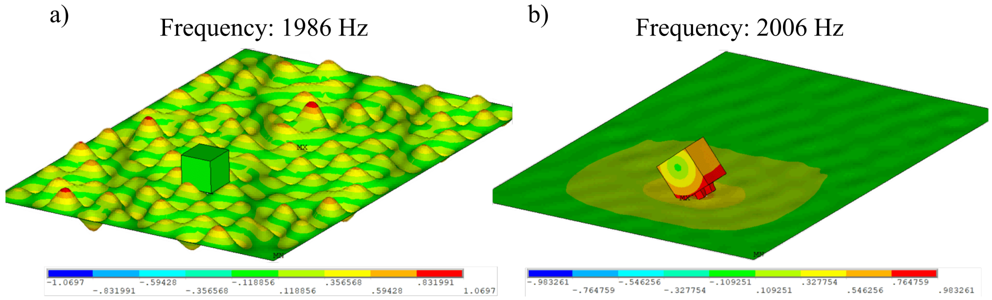

Figure 7: Depiction of the mass-normalized deformation mode: a) bending governed mode and b) complex shape mode (color online).

4.2. Source active property: $\boldsymbol{f}_2^{eq}$

The RMS values of $\boldsymbol{f}_2^{eq}$ provided by the blocked force method (see Eq. 5), for the four excitations (i.e., Excitation#1-Excitation#4), are represented in Fig. 8. The Excitation#1 provides an equivalent force mainly along the z-axis. As expected, the Excitation#4 provides the most complex dynamic behavior, involving x- and y-axis forces and moments. Only the FULL completeness allows for including all of these terms. Both Excitation#2 and #3 provide intermediate dynamic behaviors. None of the four sources generate important z-axis moment.

5. Robustness of TPA methods

The robustness of the TPA methods (i.e., their sensitivity to the model uncertainty associated with the mobility matrices completeness) is investigated in this section for multiple source active dynamic behaviors (i.e., Excitation#1-Excitation#4) and multiple matrix completenesses (i.e., FULL, OOP, TDOF and Z), in the case of the single interface point assembly and finally in the case of the four interface points assembly. As mentioned previously, boxplot representations are used to analyze the discrepancies between TPA methods' prediction of $\langle u_3^2 \rangle$ with its reference value and thus evaluate their robustness to matrix completeness.

5.1. Application to the single interface point assembly

5.1.1. FULL and OOP completenesses

The boxplots related to the FULL completeness are shown in Fig. 9 a) to d) for each source behavior. All boxplots are centered on zero regardless of

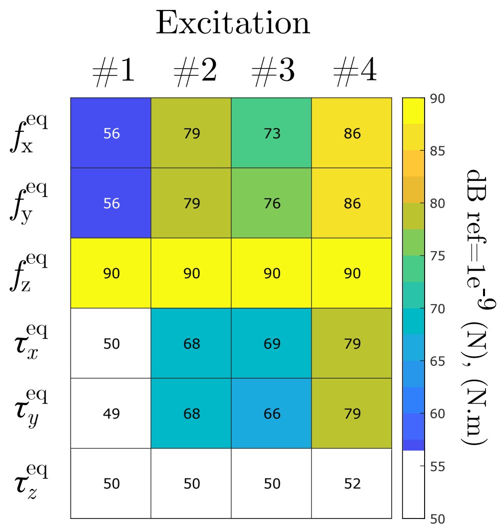

Figure 8: RMS values of $\boldsymbol{f}_2^{eq}$ terms (color online).

the excitation and the method. As expected, without any operator nor model uncertainties (the matrices are full), all TPA methods correctly predict $\langle u_3^2 \rangle$. This allows to verify the numerical application of the TPA-MI, CB-TPA and CB-TPA-DS methods related to single interface point structure.

The boxplots related to the OOP completeness are shown in Fig. 9 e) to h) for each source behavior. The TPA-MI method perfectly predicts $\langle u_3^2 \rangle$ (median and IDR are equal to zero), regardless of the complexity of the active dynamic behavior of the source. Indeed, this method is based on the receiving structure mobility ($\mathbf{Y}_{22}^B$, $\mathbf{Y}_{32}^B$ and $\mathbf{Y}_{42}^B$) and the velocities ($\boldsymbol{u}_4$) of the assembly (see Eqs. 2 and 3), which are mainly governed by bending behavior accounted for in the OOP completeness.

The CB-TPA methods provide perfect predictions of $\langle u_3^2 \rangle$ for the Excitation#1 (median and IDR are equal to zero). The prediction accuracy slightly decreases for the Excitation#2 and Excitation#3 (medians are equal to zeros and IDR are up to 1,7 dB) and for the Excitation#4 (median and IDR are respectively up to -0,2 and 8,8 dB). In order to better understand the nature of the inaccuracies affecting these predictions, the frequency-dependent $\langle u_3^2 \rangle$ estimated from the CB-TPA-FB and -IS$_P$ methods for Excitation#4 are presented in Fig. 10 (see red and orange curves respectively). It is worth noting that a linear scale for the frequency axis is used to be coherent with

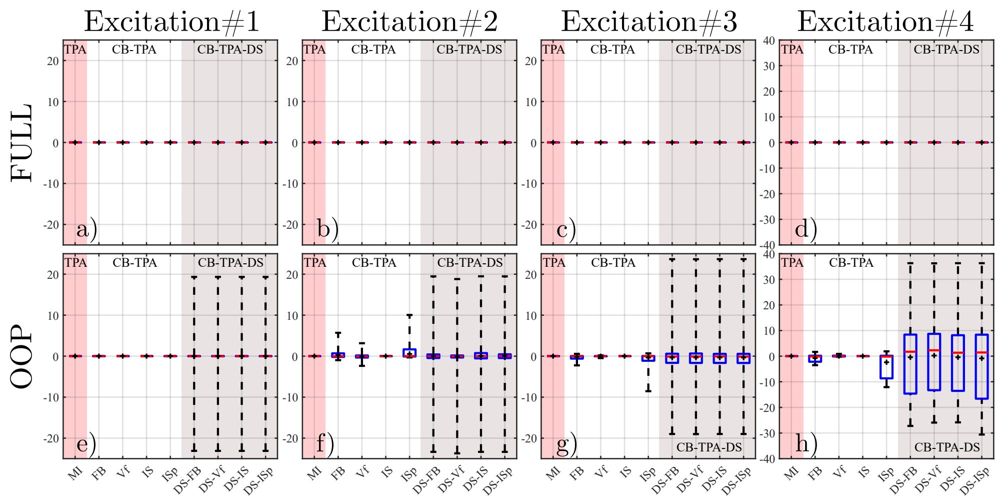

Figure 9: Boxplots representation related to Excitation#1 to Excitation#4 considering a) to d) the FULL completeness and e) to h) the OOP completeness for each TPA-MI (red frame), CB-TPA (white frame) and CB-TPA-DS (grey frame) methods applied on the single interface point structure. Note that the dynamic range is larger for d) and h) (color online).

the narrow band calculation of the statistical properties presented in the boxplots (a logarithmic scale would have overexposed the discrepancies at low frequencies). Both methods provide perfect predictions at low and medium frequencies, the assembly being bending-governed. At higher frequencies (above 1800 Hz), the predictions are less accurate. However, even in the case of CB-TPA-IS$_{\mathrm{P}}$, the prediction of $\langle u_3^2 \rangle$ is correct; 50% of the data is included between 2,2 dB (maximum value) and $-0,2$ dB (median value) of deviation from the reference. The difference between the median and mean value (-2,2 dB) highlights that the data is not evenly distributed in the boxplots (i.e., the inaccuracies are few in number but are large compared to the rest of the data). The discrepancies with the reference (black curve) are due to the omission of mobilities $Y^{AB}_{3u_z2f_x}$ and $Y^{AB}_{3u_z2f_y}$ associated to the modes with complex shapes of the assembly (see Sect. 4.1). These discrepancies at high frequencies are larger for CB-TPA-IS$_{\mathrm{P}}$, because of the incorrect characterization of $\boldsymbol{f}_2^{eq}$ which adds up to the uncertainty associated with the DoFs omission (the boxplot related to CB-TPA-FB allowing to quantify the uncertainty associated with the DoFs omission only).

According to Fig. 9.e-g), the CB-TPA-DS methods provide satisfactory

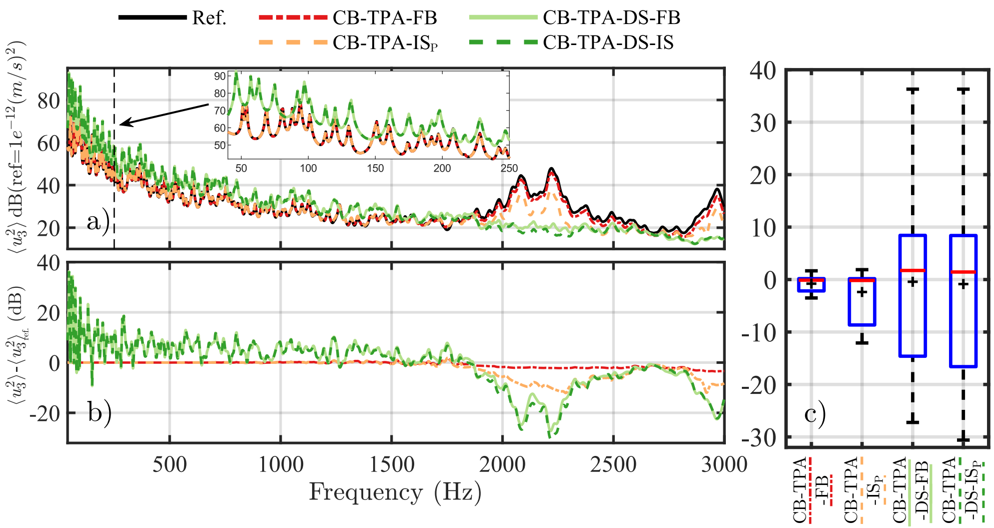

Figure 10: a) The reference and four predicted frequency-dependent $\langle u_3^2 \rangle$ provided respectively with i) CB-TPA-FB, ii) CB-TPA-IS$_{\mathrm{P}}$, iii) CB-TPA-DS-FB and iv) CB-TPA-DS-IS$_P$. b) The difference between each predicted and the reference $\langle u_3^2 \rangle$ and c) the boxplots associated to each predicted $\langle u_3^2 \rangle$. Results are provided for configuration involving Excitation#4, the OOP completeness and the single interface point structure (color online).

predictions of $\langle u_3^2 \rangle$ for Excitation#1 to Excitation#3 (median and IDR are respectively up to $-0,1$ and 2,2 dB), despite large whiskers. The size of the whiskers is due to large discrepancies at low frequencies (see zoom at low frequencies in Fig. B.15, dashed yellow line). The predictions of $\langle u_3^2 \rangle$ associated with Excitation#4 are much less accurate (median and IDR respectively up to 2,2 and 24,8 dB). The discrepancies, either at high or low frequencies, are due to the incorrect reconstruction of the coupled mobility $\mathbf{Y}_{32}^{AB}$ by the dynamic substructuring procedure. The inaccuracies are larger for a source with a complex active behavior, since more DoFs are excited (i.e., more terms of $\mathbf{Y}_{32}^{AB}$). As shown in Fig. 10 (see dark and light green curves), the two methods based on the dynamic substructuring procedure (i.e., CB-TPA-DS-FB and -IS$_P$) provide inaccurate predictions over the entire frequency range. The predictions are similar between these two CB-TPA-DS methods but different from the CB-TPA methods, suggesting that the discrepancies are mainly governed by the dynamic substructuring procedure and not by the characterization of $\boldsymbol{f}_2^{eq}$. The inaccuracies at low frequencies result from an inadequate description of the source mobility $\mathbf{Y}_{22}^{A}$

with the OOP completeness, while those at high frequencies (above 2000 Hz) result from the omission of the plate mobilities $Y^B_{2u_x 2f_x}$ and $Y^B_{2u_y 2f_y}$ (i.e., the non-consideration of the first traction compression modes of the plate).

The CB-TPA-DS methods are globally less accurate than CB-TPA (especially with the Excitation#4), suggesting the dynamic substructuring procedure may be more sensitive to the model uncertainties than the determination of $\boldsymbol{f}_2^{eq}$.

5.1.2. TDOF and Z completenesses

The boxplots related to the TDOF completeness are shown in Fig. 11.a) to d) for each source behavior. In this case, TPA-MI and CB-TPA-DS methods show a similar accuracy. They both provide satisfactory predictions of $\langle u_3^2 \rangle$ (median and IDR are respectively up to $-0,3$ and 3,6 dB), when Excitation#1 to Excitation#3 are considered. However, the predictions of $\langle u_3^2 \rangle$ are less accurate when Excitation#4 is considered (median is $-2,5$ dB lower and IDR is 15,7 dB larger). The observed discrepancies are mainly due to the plate mobilities required in these TPA methods (i.e., $\mathbf{Y}^B_{22}$ and $\mathbf{Y}^B_{32}$) and which are not well described by the translational DoFs.

CB-TPA generally provides better predictions of $\langle u_3^2 \rangle$ than TPA-MI and CB-TPA-DS methods. Indeed, the modes with complex shapes of the assembly appearing at high frequencies (f >2000 Hz) could be partially described with the terms $Y^{AB}_{3u_z 2f_x}$ and $Y^{AB}_{3u_z 2f_y}$. The discrepancies affecting the CB-TPA methods mostly come from bending modes at low to mid frequencies (f <2000 Hz) and which are not well accounted for by the TDOF completeness. These inaccuracies are larger for a source with a complex active behavior involving x- and y-axis moments, such as Excitation#4, since the TDOF completeness does not allow to account for these moments related to the bending motion.

The boxplots related to the Z completeness are shown in Fig. 11.e) to h) for each source behavior. For both the TPA-MI and CB-TPA-DS methods, the boxplots associated with the Z completeness are similar to those associated with the TDOF completeness, suggesting that the consideration of mobilities related to x- and y-axis translational DoFs do not significantly improve the predictions of $\langle u_3^2 \rangle$ provided by these methods. In contrast, for the CB-TPA methods, the boxplots associated with the Z completeness are larger when compared to the TDOF completeness, especially for Excitation#4 (IDR are 12 dB larger). Indeed, the modes with complex shapes at high frequencies might be partially described with the x- and y-axis translational DoFs, and which should not be discarded.

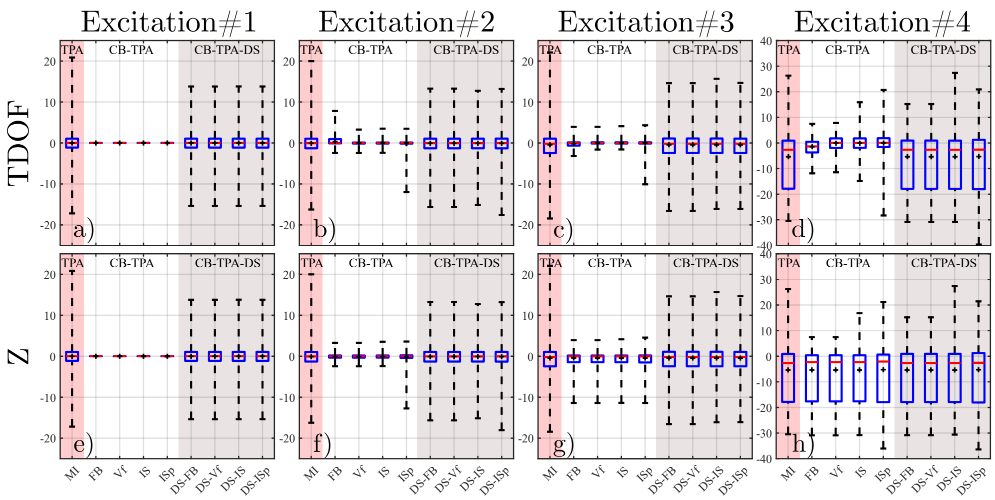

Figure 11: Boxplots representation related to Excitation#1 to Excitation#4 considering a) to d) the TDOF completeness and e) to h) the Z completeness for each TPA-MI (red frame), CB-TPA (white frame) and CB-TPA-DS (grey frame) methods applied on the single interface point structure. Note that the dynamic range is larger for d) and h) (color online).

In order to better understand the nature of the inaccuracies affecting these predictions, the frequency-dependent $\langle u_3^2 \rangle$ related to the CB-TPA-IS and CB-TPA-DS-IS methods with both TDOF and Z completenesses for Excitation#4 are presented in Fig. 12. CB-TPA-IS with both TDOF and Z completenesses (red and orange curves) provide same predictions at low and mid frequencies, suggesting that the x- and y-axis mobilities do not have significant influence for describing the bending modes of the assembly. However, accounting for x- and y-axis translational DoFs leads to better predictions above 2000 Hz, resulting in an IDR 14,3 dB smaller for the TDOF completeness than the Z. Consequently, the TDOF completeness seems acceptable to describe these modes with complex shapes.

CB-TPA-DS-IS with both TDOF and Z completenesses lead to the same predictions in the entire frequency range (see light and dark green curves). The results are similar to those provided by CB-TPA-IS with Z completeness above 2000 Hz (see orange curve), suggesting that the TDOF and Z completenesses do not allow for reconstructing modes with complex shape by the dynamic substructuring procedure.

In agreement with the literature, modes with complex shape appear at high frequencies for the considered assembly [17, 18, 20]. However, the conclusions slightly differ regarding the influence of rotational DoFs omission on the TPA methods prediction accuracy, probably because the dynamic behavior of the structure considered in this work is different from those investigated in the aforementioned studies [17, 18, 20]. In these works, it has been suggested that the influence of rotational DoFs is significant at high frequencies, due to modes with complex shape, and that they should be accounted for in the TPA or dynamic substructuring equations. In this study, exploiting a plate bending-governed at low frequencies as receiving structure, the omission of rotational DoFs prevent correct predictions of the bending modal behavior of the structure, especially at low frequencies, when a source with complex active dynamic behavior is considered. In contrast, in the case of the CB-TPA methods, the modes with complex shape at high frequencies are acceptably described by the TDOF completeness.

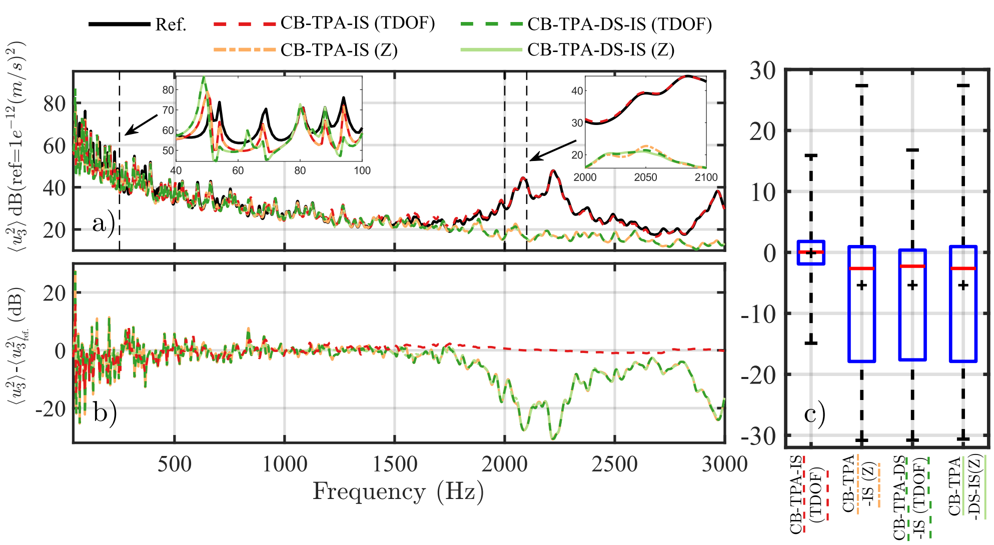

Figure 12: a) The reference and four predicted $\langle u_3^2 \rangle$ provided respectively with i) CB-TPA-IS and TDOF completeness, ii) CB-TPA-IS and Z completeness, iii) CB-TPA-DS-IS and TDOF completeness and iv) CB-TPA-DS-IS and Z completeness. b) The difference between each predicted and the reference $\langle u_3^2 \rangle$ and c) the boxplots associated to each predicted $\langle u_3^2 \rangle$. Results are provided for configuration involving Excitation#4, the TDOF or Z completeness and the single interface point structure
(color online)

5.2. Application to the four interface points assembly

Boxplot representations are also used to evaluate the robustness of each method applied to the four interface points assembly (see Fig. 3). The boxplots are shown in Fig. 13 for each source behavior and the OOP, TDOF and Z completenesses. The boxplots related to the FULL completeness are not shown, since the $\langle u_3^2 \rangle$ is perfectly predicted similarly to the case of the single interface point structure (see Fig. 9.a-d).

The accuracy of the TPA-MI method is similar to the one already observed for the single interface configuration: the OOP completeness allows perfect predictions of $\langle u_3^2 \rangle$ and on the contrary, the TDOF and Z completenesses provide inaccurate predictions of $\langle u_3^2 \rangle$ (median down to $-4,5$ dB and IDR up to 13,9 dB, see Fig. 13.f) and j)) due to the bending-governed mobility $\mathbf{Y}_{32}^B$. The TPA-MI method accuracy is weakly dependent on the active behavior of the source as well as on the consideration of the x- and y-axis translational DoFs.

The accuracy of CB-TPA methods improves in the case of the four interface points configuration, compared to the single interface point configuration. The $\langle u_3^2 \rangle$ is correctly predicted with the OOP, TDOF and Z completenesses. Only few discrepancies can be observed mainly for the CB-TPA-IS$_\mathrm{P}$ method in the case of the Excitation#2 (see Fig. 13.b) and j)), but could be considered as acceptable (50% of the data are including between -1,6 et 0 dB, since the median is equal to 0, see Fig. 13.f)). The fairly good accuracy provided by the Z completeness can be attributed to an implicit consideration of the global rotations along the x- and y-axis thanks to the assessment of the z-axis translational DoFs at the four interface points (in the similar way to the equivalent multi-point connection method described in [37]). This implicit consideration is allowed here, since the assembly does nearly not deform between the four interface points. The predictions are more accurate for the TDOF completeness (median equal to 0 and IDR less than 0,3 dB) than for the Z completeness, since all of the TDOF are considered as well as the implicit consideration of all the global rotation of the source.

The CB-TPA-DS methods provide the less accurate predictions. Their accuracy is found to be similar to the one already observed in the case of the single interface configuration, except for Excitation#3 and TDOF completeness (i.e., Fig. 13.h)). The predictions of $\langle u_3^2 \rangle$ are correct as long as (i) the OOP completeness is used and (ii) the source shows a relatively simple active dynamic behavior (i.e., Excitation#1 to Excitation#3). Otherwise the predictions of $\langle u_3^2 \rangle$ are inaccurate (median and IDR are respectively up

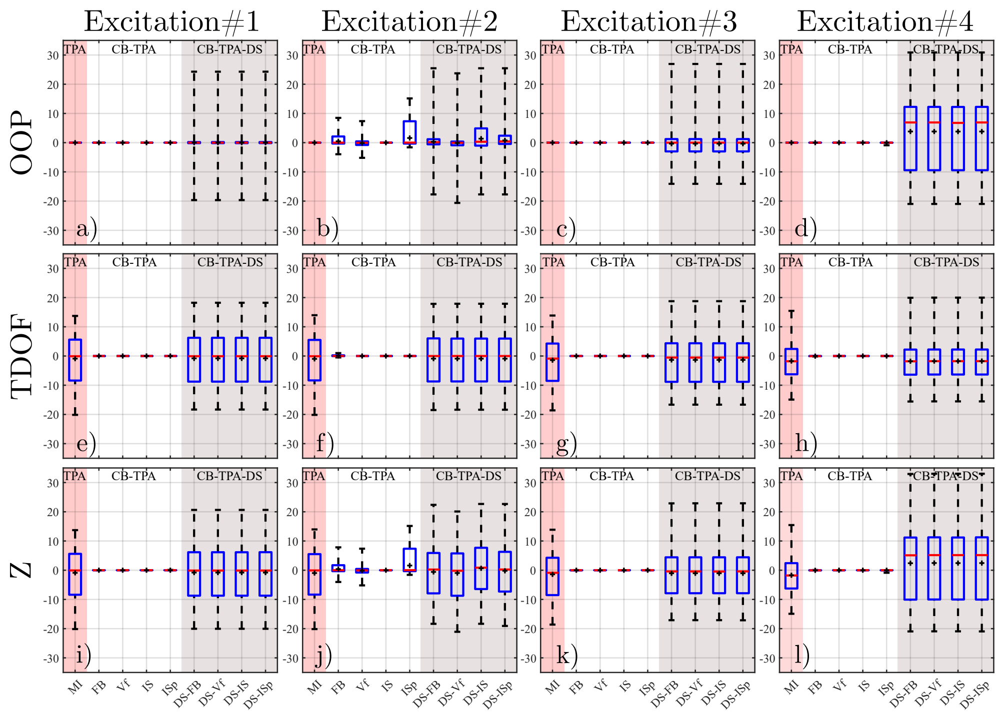

Figure 13: Boxplots representation related to Excitation#1 to Excitation#4 considering a) to d) the OOP completeness, e) to h) the TDOF completeness and i) to l) the Z completeness for each TPA-MI (red frame), CB-TPA (white frame) and CB-TPA-DS (grey frame) methods applied on the four interface points structure (color online).

to 6,9 and 21,7 dB). Again, the dynamic substructuring procedure appears to be a sensitive step since it requires the mobilities of both components, especially for sources with complex dynamic behavior such as Excitation#4 (see Fig. 13.d) and l)).

Additional investigations are presented in the Appendix C, considering a small plate as receiving structure (refer to as B^*). The results lead to similar conclusions than those presented in Fig. 13 in the case of the large plate B, except for the OOP completeness. The latter completeness allows the CB-TPA-DS methods to provide accurate predictions, since the assembly AB^* does not involve modes with complex shape at high frequency.

6. Conclusion

The TPA methods attracted a lot of attention in the last few years to investigate and mitigate structure borne noise, but their use is still restricted due to model uncertainties such as the determination of mobilities related to rotational DoFs or in-plane DoFs, which are generally omitted for convenience purpose. However, this approximation may lead to significant inaccurate predictions.

In this work, the sensitivity of nine TPA methods to the mobility matrices completeness has been numerically investigated for several configurations of assemblies (i.e., different active source properties, different numbers of contact points). The investigations are conducted on a numerical model of a rigid source attached to a thin plate, designed to mimic the dynamic behavior of an aircraft light equipment attached to an aircraft-like structure. Four mobility matrix completenesses and four source active dynamic behaviors are considered and the TPA methods are applied on assemblies based on one or four interface points. A boxplot representation is introduced and used to evaluate the TPA method's robustness with respect to the completeness and the active dynamic behavior of the source.

It is shown that, the required completeness depends on the TPA method considered and on the active and passive dynamic behavior of the structures. In this study, the classical TPA-MI method leads to perfect predictions with the FULL and OOP completenesses, for both the four and single interface point assembly, since they are suitable for describing the bending-governed dynamic behavior of the considered receiving structure. In contrast, the TDOF and Z completeness allow correct predictions only when a source with a simple active dynamic behavior (e.g., Excitation#1 in this study) and a unique interface point assembly are involved. The CB-TPA methods lead to almost perfect predictions for the four interface point assembly, regardless of the completeness. This accuracy is allowed by an implicit consideration of the rotations by the translations (thanks to the rigid behavior between the four points of interface induced by the source). In the case of the single interface point assembly, the OOP and TDOF completenesses provide correct predictions, but their accuracy decreases as the active behavior of the source becomes more complex. The CB-TPA methods appear thus as complementary methods to the TPA-MI method for validation purposes. In contrast, the CB-TPA-DS methods provide generally the less accurate predictions, especially for the source with a complex active dynamic behavior. Going through FULL completeness appears as a requirement for robust predictions with these methods, since it is the only one of the four investigated completeness suitable for describing the mobility of both components considered in this work.

This study has underlined the DoFs to consider for a robust application of multiple TPA methods on typical aeronautical assemblies. Although the study is conducted considering multiple TPA methods, active behaviors and assembly configurations to be comprehensive, the conclusions are, however, limited to the considered models or similar, namely a rigid source hard mounted on a bending-governed receiving structure. The consideration of soft-mounted assembly or the brackets of hydraulic pipes as case studies is perspective of the current work.

7. Acknowledgements

This work has been supported by (alphabetically ordering) Bell Textron Canada limited, Bombardier Aerospace, CRIAQ (Consortium for Research and Innovation in Aerospace in Canada), NSERC (Natural Sciences and Engineering Research Council of Canada) and Parker Hannifin Corporation. Images are used courtesy of ANSYS, Inc.

Appendix A. Influence of the target point location

A common practice, according to the literature, consists in using a single target point as the objective indicator to evaluate the robustness of a TPA method's prediction. To evaluate the influence of the target point location on the evaluation of a method robustness, the RMS values of the difference between the reference and the target velocities, provided by the CB-TPA-IS method, have been computed at each target location considered in this work (n_3=1408, see Sect.3.4). The difference between the RMS values of the predicted and reference velocities (in dB) is shown in Fig. A.14 a) and b) respectively when the FULL and Z completenesses are considered. Results related to Fig. A.14 b) show that the difference of the RMS value is not homogeneous on the surface of the plate when Z completeness is considered for the velocity predictions, suggesting a possible dependence of the CB-TPA-IS method reliability according to the target point location on the receiving structure. Going through spatial averages appears as a requirement for robust predictions of methods reconstruction capabilities.

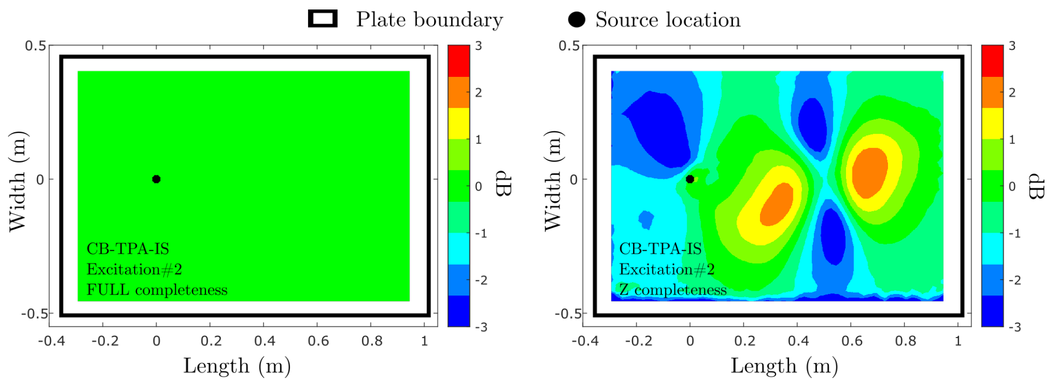

Figure A.14: Difference between the RMS value of the reference and the RMS value of predicted velocity using CB-TPA-IS method considering a) FULL and b) Z completenesses (color online).

Appendix B. On the use of statistical representation to quantify the TPA methods accuracy

In this appendix, three predictions of the reference $\langle u_3^2 \rangle$ from TPA methods are detailed in order to illustrate the boxplot representation. They are associated with (i) a perfect prediction of $\langle u_3^2 \rangle$, (ii) a prediction leading to large whiskers and (iii) a prediction leading to large whiskers and IDR. The predictions have been obtained using the CB-TPA-IS and CB-TPA-DS-IS methods applied to the single interface point assembly and considering the Excitation#1.

Fig. B.15.a) presents the reference frequency-dependent $\langle u_3^2 \rangle$ and three predictions provided by (i) the CB-TPA-IS method with the OOP completeness (dashed red line), (ii) CB-TPA-DS-IS method with the OOP completeness (dashed orange line) and (iii) the CB-TPA-IS method with the TDOF completeness (dashed green line). The frequency-dependent difference between each TPA prediction and the reference is shown in Fig. B.15.b) and the associated boxplots are shown in Fig. B.15.c).

The CB-TPA-IS method with OOP completeness (dashed red curves) provides perfect prediction of $\langle u_3^2 \rangle$. This perfect prediction is captured by the boxplot representation: the median and IDR are equal to 0 dB.

The CB-TPA-DS-IS method with the OOP completeness (dashed orange curves) provides almost perfect prediction of $\langle u_3^2 \rangle$ (the median and IDR equal to 0 dB), despite large whiskers. The size of the whiskers is due to the

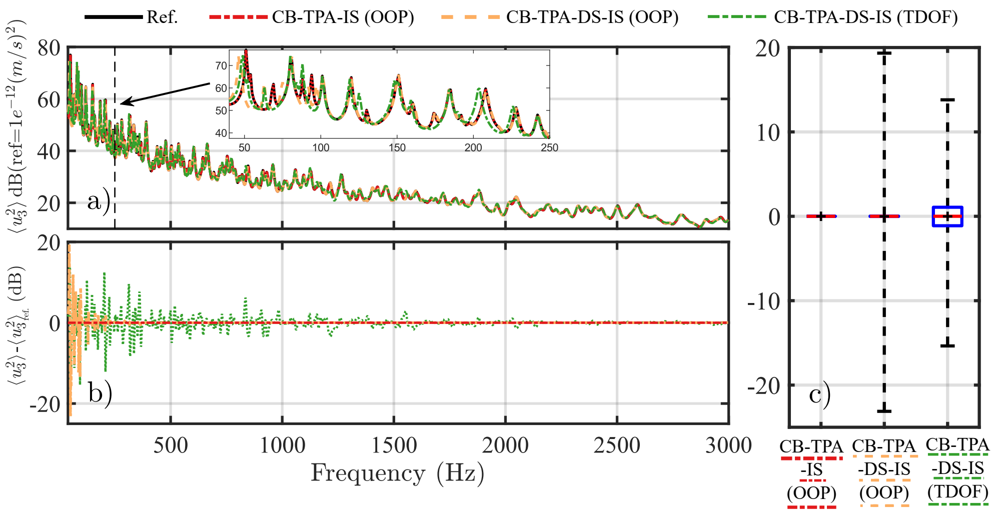

Figure B.15: a) The reference and three predicted $\langle u_3^2 \rangle$ related to Excitation#1 and provided respectively with (i) OOP completeness and CB-TPA-IS method, (i) OOP completeness and CB-TPA-DS-IS method and (iii) TDOF completeness and CB-TPA-IS method. b) the difference between each predicted and the reference $\langle u_3^2 \rangle$ and c) the boxplots associated to each predicted $\langle u_3^2 \rangle$. Results are pertaining to the single interface point configuration assembly (color online).

inaccuracies located to a narrow frequency range at low frequencies (below 150Hz), which are due to the incorrect description of the source mobility $\mathbf{Y}_{22}^{A}$ required for the dynamic substructuring procedure.

The CB-TPA-IS method with TDOF (dark green curves) completeness provides a good prediction of $\langle u_3^2 \rangle$ (the median and IDR respectively equal to 0 and 2,2 dB). The IDR is larger than with the OOP completeness, since a larger frequency range is affected by inaccuracies.

Appendix C. Influence of the receiving structure on the TPA robustness

This study evaluates the influence of the dynamic behavior of the receiving structure on the TPA methods predictions. The four interface points source A is attached to a plate B^*, which is designed to avoid traction-compression modes in the considered frequency range. Its dimensions are $(210 \times 190 \times 1,5\ \text{mm}^3)$ and simply supported condition are imposed at the edges of B^*. The material properties are the same than the ones used for the plate B. The geometry of the assembly AB^* is shown in Fig. C.16.

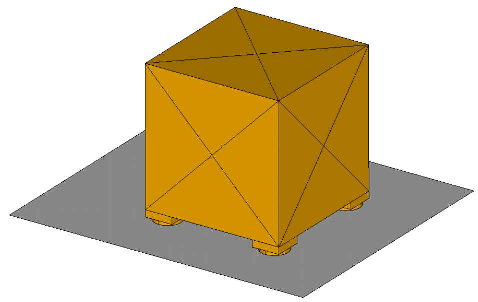

Figure C.16: Geometries of the assembly AB^*.

The boxplots associated with the TPA methods applied to the AB^* assembly are presented in Fig. C.17, for each active behavior of the source. The boxplots associated with the FULL completeness are not shown because the response $\langle u_3^2 \rangle$ is again perfectly estimated. The observations for the TPA-MI and CB-TPA methods are exactly the same as for the assembly AB .

In the case of the CB-TPA-DS methods, the observations are slightly different. These methods estimate more accurately $\langle u_3^2 \rangle$ with OOP completeness when they are applied to the assembly AB^* (IDRs are down to 22,1 dB smaller) than to AB (see Fig. 13))), especially in the case Excitation#4. this difference was expected, since AB^* does not have complex shape modes at high frequencies unlike to AB.

Regarding the TDOF completenesses, the CB-TPA-DS methods do not provide accurate estimations of $\langle u_3^2 \rangle$ (as observed for the assembly AB). The inaccuracies are due to a frequency shift of the peaks of $\langle u_3^2 \rangle$. These shifts lead to as many overestimations as underestimations, which is reflected on the boxplots by large IDRs (reaching 13,5 dB), but with mean and median values close to zero. The frequency shifts being due to an unsuitable reconstruction of the dynamic behavior of the assembly AB^* by DS. Note that similar observations have been established at low frequencies (below 800 Hz) for the single interface point assembly AB (see Fig. 12). The results were therefore expected and support the hypothesis that TDOF completeness is not suitable for the application of CB-TPA-DS methods to a bending-governed receiving structure.

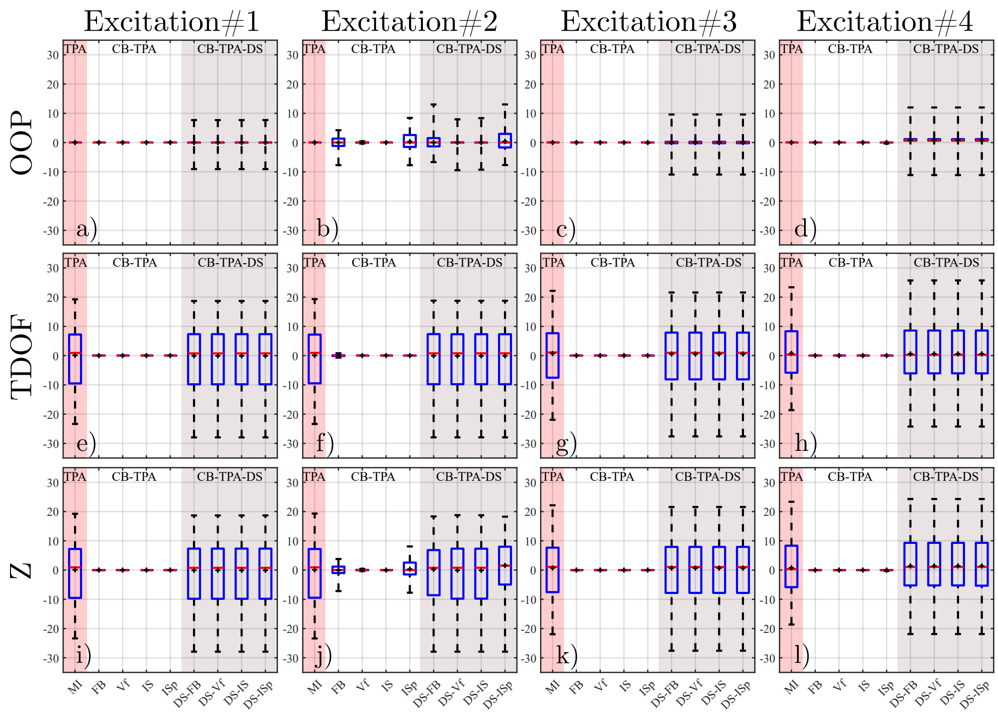

Figure C.17: Boxplots representation related to Excitation#1 to Excitation#4 considering a) to d) the OOP completeness, e) to h) the TDOF completeness and i) to l) the Z completeness for each TPA-MI (red frame), CB-TPA (white frame) and CB-TPA-DS (grey frame) methods applied on the four interface points structure $B*$ (color online).

Appendix D. Comparison between the numerical model and industrial structures

The mobilities of two industrial aeronautical hydraulic pumps have been measured according to a TDOF completeness and are compared to those of the 4 interface points cubic source. The results are presented considering mobilities relative to to one of the four interface points. The magnitudes of the mobilities Y^A_{2ux2fx}, Y^A_{2uy2fy} and Y^A_{2uz2fz} are shown respectively in Fig. D.18.a), b). and c)., together with the mobilities related of the 4 interface points cubic source.

The cubic source has a dynamic behavior close to that of hydraulic pumps (i.e., low modal density). The magnitude of their mobilities are similar to those of the cubic source.

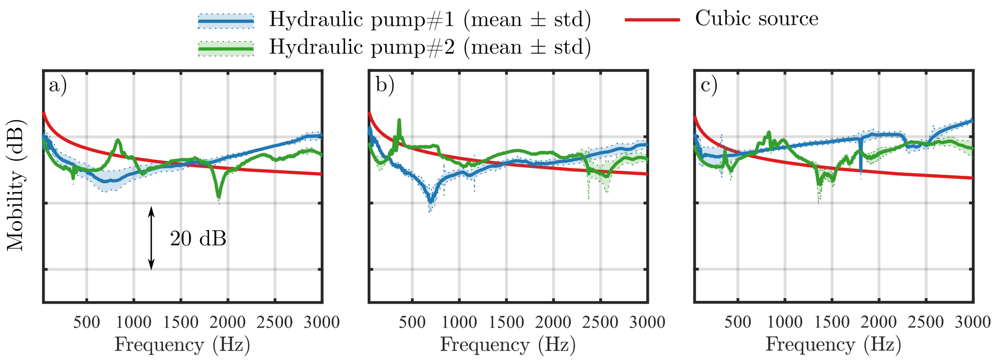

Figure D.18: a) Y^A_{2ux2fx}, b) Y^A_{2uy2fy} and c) Y^A_{2uz2fz} mobilities measured on two industrial hydraulic pumps (blue and green lines) and simulated on the 4 interface points numerical model (red line).

The mobilities of two structures from distinct aircraft have been measured, considering the translational DoF normal to the surface only. The magnitude of these mobilities are shown in Fig. D.19, together with the mobilities Y^B_{2uz2fz} of the aluminium plates B and $B*$. The results show similar magnitudes between the mobilities of the aircraft structures and both aluminium plates considered in this work. The aircraft structures have modal densities closer to that of the smallest plate (orange curve), but the local variations of amplitudes are closer to that of the largest plate (red curve).

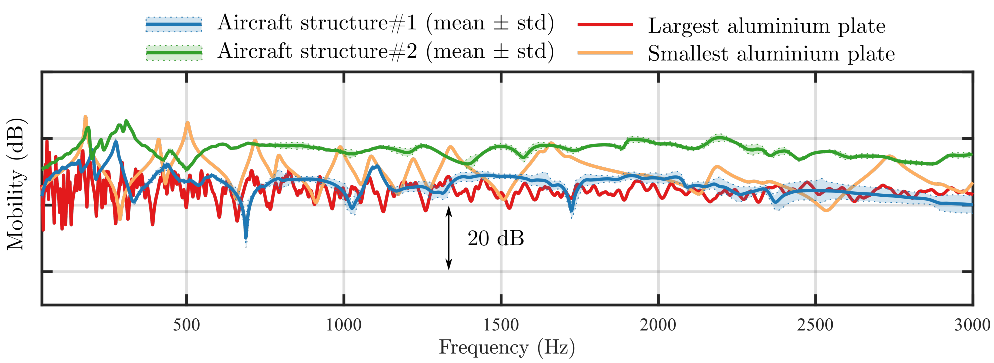

Figure D.19: Y^B_{2uz2fz} mobility measured on two distinct aircraft structures (blue and green lines) and simulated on the numerical models of the aluminium plates (red and orange lines).

References

[1] Lai, H. K., Moorhouse, A., and Gibbs, B. *Experimental round-robin evaluation of structure-borne sound source force-power test methods.* Noise Control Engineering Journal, 2016, vol. 64, no 2, p. 170-180.

[2] Fiorentin, T. A., Ferguson, N. S., Renno, J. M., and Lenzi, A. *Structural response of an aircraft fuselage to hydraulic system-A wave and mobility approach.* Noise Control Engineering Journal, 2013, vol. 61, no 1, p. 87-99.

[3] van der Seijs, M. V., de Klerk, D., and Rixen, D. J., *General framework for transfer path analysis: History, theory and classification of techniques.*, Mechanical Systems and Signal Processing, 2016, vol. 68, p. 217-244.

[4] van der Seijs, M. V., Pasma, E. A., van den Bosch, D. D., and Wernsen, M. W. F., *A benchmark structure for validation of experimental substructuring, transfer path analysis and source characterisation techniques.* In : Dynamics of Coupled Structures, Volume 4. Springer, Cham, 2017. p. 295-305.

[5] de Klerk, D., Rixen, D. J., and Voormeeren, S. N., *General framework for dynamic substructuring: history, review and classification of techniques.* AIAA journal, 2008, vol. 46, no 5, p. 1169-1181.

[6] Moorhouse, A. T., Elliott, A. S., and Evans, T. A. *In situ measurement of the blocked force of structure-borne sound sources.* Journal of Sound and Vibration, 2009, vol. 325, no 4-5, p. 679-685.

[7] ISO TC-43 / NWIP 21955 *Vehicles — Experimental method for transposition of dynamic forces generated by an active component from a test bench to a vehicle.* International Organization for Standardization, 2016.

[8] Allen, M. S., Rixen, D., Van der Seijs, M., Tiso, P., Abrahamsson, T., and Mayes, R. L. *Substructuring in Engineering Dynamics.* Springer International Publishing, 2020.

[9] Meggitt, J. W. R., Moorhouse, A. T., and Elliott, A. S. *A covariance based framework for the propagation of uncertainty through inverse problems with an application to force identification.* Mechanical Systems and Signal Processing, 2019, vol. 124, p. 275-297.

[10] Meggitt, J. W. R., Moorhouse, A. T., and Elliott, A. S. *On the completeness of interface descriptions and the consistency of blocked forces obtained in situ.* Mechanical Systems and Signal Processing, 2020, vol. 145, p. 106850.

[11] Meggitt, J. W. R., Moorhouse, A. T., Wienen, K., et al. *A framework for the propagation of uncertainty in Transfer Path Analysis.* Journal of Sound and Vibration, 2020, vol. 483, p. 115425.

[12] van den Bosch, D., van der Seijs, M., de Klerk, D. *A comparison of two source characterisation techniques proposed for standardisation.* SAE International Journal of Advances and Current Practices in Mobility, 2019, vol. 1, no 2019-01-1540, p. 1755-1765.

[13] Lennström, D., Olsson, M., Wullens, F., and Nykänen, A. *Validation of the blocked force method for various boundary conditions for automotive source characterization.* Applied Acoustics, 2016, vol. 102, p. 108-119.

[14] Chen, K. and Herrin, D. W. *Blocked force determination on plate structures using an offset interface.* Applied Acoustics, 2020, vol. 158, p. 107044.

[15] de Klerk, D., Rixen, D., Voormeeren, S. N., and Pasteuning, F. *Solving the RDoF problem in experimental dynamic substructuring.* In : Proceedings of the Twentysixth International Modal Analysis Conference, Orlando, FL. 2008.

[16] O. Almiròn, J., Bianciardi, F., Corbeels, P., and Desmet, W. *Predicting vibration levels on an experimental test case by using invariant loads (eg blocked forces) as source characterization.* In : Proceedings of ISMA 2018-International Conference on Noise and Vibration Engineering and USD 2018-International Conference on Uncertainty in Structural Dynamics. KU Leuven, 2018. p. 4131-4145.

[17] Haeussler, M., Mueller, T., Pasma, E. A., Freund, J., Westphal, O., and Voehringer, T. *Component TPA: benefit of including rotational degrees of freedom and over-determination.* ISMA 2020-International Conference on Noise and Vibration Engineering. 2020. p. 1135-1148.

[18] van der Seijs, M. V., de Klerk, D., Rixen, D. J., et al. *Validation of current state frequency based substructuring technology for the characterisation of steering gear–vehicle interaction.* Topics in Experimental Dynamic Substructuring, Volume 2. Springer, New York, NY, 2014. p. 253-266.

[19] Pavić, G., Sandier, C., et Carniel, X. *Characterisation of a small vibration source.* Proceeding ISMA 2014, 2014, p. 15-17.

[20] Duarte, M. L. M. et Ewins, D. J *Some insights into the importance of rotational degrees-of-freedom and residual terms in coupled structure analysis.* Proceeding of the international society for optical engineering. Spie International Society for Optical, 1995. p. 164 - 170.

[21] Gialamas, T., Tsahalis, D., Bregant, L., et al. *Substructuring by means of FRFs: some investigations on the significance of rotational DOFs.* Proceeding of the international society for optical engineering. Spie International Society for Optical, 1996. p. 619 - 625.

[22] Liu, W. et Ewins, D. *The importance assessment of RDOF in FRF coupling analysis.* Proceedings of the Seventeenth International Modal Analysis Conference. 1999. p. 1481-1487.

[23] Campbell, R. L. et Hambric, S. A. *Application of Frequency Domain Substructure Synthesis Technique for Plates loaded with Complex Attachments.* Pennsylvania State University Park applied research Lab, 2004

[24] Elliott, A., Moorhouse, A., Meggitt, J. *Identification of coupled degrees of freedom at the interface between sub-structures.* INTER-NOISE and NOISE-CON Congress and Conference Proceedings. Institute of Noise Control Engineering, 2018. p. 672-680.

[25] Helderweirt, S., van der Auweraer, H., Mas, P., et al. *Application of accelerometer-based rotational degree of freedom measurements for engine subframe modelling.* Proceeding of IMAC-XIX: A Conference on Structural Dynamics,. 2001. p. 1298-1304.

[26] Prenant, S., Rolland, V., Padois, T., Chérif, R., Etchessahar, M., Klop, R., ... and Doutres, O. *Using transfer path analysis methods for assessing*

the velocity response on a plate generated by a dummy vibratory source. Proceeding of ICSV26, 2019.

[27] Elliott, A. S., Moorhouse, A. T., Huntley, T., et al. *In-situ source path contribution analysis of structure borne road noise.* Journal of Sound and Vibration, 2013, vol. 332, no 24, p. 6276-6295.

[28] Allemang, Randall J. *The modal assurance criterion–twenty years of use and abuse.* Sound and vibration, 2003, vol. 37, no 8, p. 14-23.

[29] Petersen, K. B., Pedersen, M. S. *The matrix cookbook.* Technical University of Denmark, 2008, 7(15), 510.

[30] Lai, H. Y. *Alternative test methods for measuring structure-borne sound power.* Proceeding of INTER-NOISE and NOISE-CON Congress and Conference. Institute of Noise Control Engineering, 2006. p. 2515-2524.

[31] Wernsen, M. W. F., van der Seijs, M. V., and Klerk, D. D. *An indicator sensor criterion for in-situ characterisation of source vibrations.* In : Sensors and Instrumentation, Volume 5. Springer, Cham, 2017. p. 55-69.

[32] Ansys Technical documentation *ANSYS Mechanical APDL Command Reference.* Release 13.0 , 2010.

[33] Klop, R. J. *Investigation of hydraulic transmission noise sources.* PhD thesis, Purdue University, USA, 2010.

[34] Cremer, L. et Heckl, M. *Structure-borne sound: structural vibrations and sound radiation at audio frequencies.* Springer Science and Business Media, 2013.

[35] Venugopal, H. *Component-Based Transfer Path Analysis and Hybrid Substructuring at high frequencies: A treatise on error modelling in Transfer Path Analysis.* Master thesis, KTH Royal Institute of Technology, Sweden, 2020.

[36] Kohrmann, M. *Numerical methods for the vibro-acoustic assessment of timber floor constructions.* PhD thesis, Technische Universität München, Germany, 2017.

[37] D'Ambrogio, W., et Sestieri, A. *A unified approach to substructuring and structural modification problems.* Shock and Vibration, 2004, vol. 11, no 3, 4, p. 295-309.